

# C-Axis Tunneling Spectra in High- $T_c$ Superconductors in the Presence of a d Charge-Density Wave

A. Greco<sup>a,b</sup> and R. Zeyher<sup>a</sup>

<sup>a</sup> *Max-Planck-Institut für Festkörperforschung,  
Heisenbergstr.1, 70569 Stuttgart, Germany*

<sup>b</sup> *Permanent address: Departamento de Física, Facultad de Ciencias Exactas e Ingeniería and  
IFIR(UNR-CONICET), Av. Pellegrini 250, 2000-Rosario, Argentina*

(November 16, 2018)

The optimally doped and underdoped region of the  $t - J$  model at large  $N$  ( $N$  is the number of spin components) is governed by the competition of d-wave superconductivity (SC) and a d Charge-Density Wave (d-CDW). The partial destruction of the Fermi surface by the d-CDW and the resulting density of states are discussed. Furthermore, c-axis conductances for incoherent and coherent tunneling are calculated, considering both an isotropic and an anisotropic in-plane momentum dependence of the hopping matrix element between the planes. The influence of self-energy effects on the conductances is also considered using a model where the electrons interact with a dispersionless, low-lying branch of bosons.

We show that available tunneling spectra from break-junctions are best explained by assuming that they result from incoherent tunneling with a strongly anisotropic hopping matrix element of the form suggested by band structure calculations. The conductance spectra are then characterized by one single peak which evolves continuously from the superconducting to the d-CDW state with decreasing doping. The intrinsic c-axis tunneling spectra are, on the other hand, best explained by coherent tunneling. Calculated spectra show at low temperatures two peaks due to SC and d-CDW. With increasing temperature the BCS-like peak moves to zero voltage and vanishes at  $T_c$ , exactly as in experiment. Our results thus can explain why break junction and intrinsic tunneling spectra are different from each other. Moreover, they support a scenario of two competing order parameters in the underdoped region of high- $T_c$  superconductors.

## I. INTRODUCTION

One important topic in high- $T_c$  superconductors is the question of how many order parameters are needed for a proper description of the optimally doped and underdoped cases. One scenario assumes that only the superconducting order parameter is relevant. The decrease in the transition temperature  $T_c$  is then caused by fluctuations of its phase and the pseudogap is locally just the superconducting gap. A second scenario assumes that the physics in the underdoped and optimally doped region is mainly determined by the competition of the superconducting order parameter with a second one in the particle-hole channel. Examples could be the antiferromagnetic, s- and d- charge density wave or stripe order parameters.

Many experiments such as angle-resolved photoemission [1] or tunneling in break-junctions [2–5] suggests that there is only one energy scale related with the gap and that this scale increases monotonically with decreasing doping. Recent intrinsic c-axis tunneling spectra in several cuprates [6–13] seem to modify this picture. Optimally doped or underdoped samples show at low temperatures two peaks for positive or negative voltages. The peak at larger voltages stays essentially at the same position, but becomes broader with increasing temperature.

With decreasing doping it moves towards larger voltages. Though this peak behaves similar to the one seen in tunneling in break-junctions, it has recently been argued that heating effects could seriously affect this peak [14,15]. The peak at smaller voltages moves towards zero voltage with increasing temperature, loses hereby intensity and vanishes at  $T_c$ . Heating effects should be unimportant for the behavior of this peak. Intrinsic tunnel spectra of this kind have been found both for double layer and as well as single layer materials [12]. On the other hand, strongly overdoped samples show only one sharp peak with properties as expected from BCS theory [6].

It is tempting to associate the two peaks observed in the optimally doped and the underdoped region with the SC and the pseudogap, as has been done in some of the above references. In the following we will investigate whether the widely accepted  $t - J$  model supports such a picture. To this end we will present calculations for the conductance based on a  $t$ - $J$  model where the two spin components have been generalized to  $N$  components and the leading diagrams at large  $N$  are taken into account. As discussed in detail in Ref. [16] the phase diagram in this limit has a quantum critical point (QCP) separating at  $T=0$  the normal phase at large dopings from a d-CDW state at lower dopings if superconductivity is omitted.

Allowing also for superconductivity the QCP separates a pure superconducting state from a ground state containing both superconductivity and a d-CDW. The properties at optimal doping and in the underdoped regime are mainly determined by the competition between superconductivity and the d-CDW. This model thus represents an example for the above second scenario.

## II. DENSITY OF STATES AND FERMI SURFACE IN THE PRESENCE OF SC AND D-CDW

The d-CDW order parameter, appropriate for the  $t$ - $J$  model at large  $N$ , is given by  $\Phi(\mathbf{k}) = -i/2N_c \sum_{\mathbf{q}\sigma} J(\mathbf{k} - \mathbf{q}) \langle \tilde{c}_{\mathbf{q}\sigma}^\dagger \tilde{c}_{\mathbf{q}+\mathbf{Q}\sigma} \rangle$ .  $J$  is the Heisenberg coupling,  $\tilde{c}^\dagger, \tilde{c}$  are creation and annihilation operators for electrons under the constraint that double occupancies of lattice sites are excluded,  $N_c$  is the number of primitive cells,  $\langle \dots \rangle$  denotes an expectation value, and  $\mathbf{Q}$  is the wave vector of the d-CDW. Keeping only the instantaneous term in the effective interaction, the superconducting order parameter is  $\Delta(\mathbf{k}) = 1/2N_c \sum_{\mathbf{q}} (J(\mathbf{k} - \mathbf{q}) - V_C(\mathbf{k} - \mathbf{q})) \langle \tilde{c}_{\mathbf{q}\uparrow} \tilde{c}_{-\mathbf{q}\downarrow} \rangle$ . As shown in Ref. [16] it is in general necessary to include the Coulomb potential  $V_C$  in order to stabilize the d-CDW with respect to phase separation. In the presence of the two order parameters the operators  $(\tilde{c}_{\mathbf{k},\uparrow}^\dagger, \tilde{c}_{-\mathbf{k},\downarrow}, \tilde{c}_{\mathbf{k}+\mathbf{Q},\uparrow}^\dagger, \tilde{c}_{-\mathbf{k}-\mathbf{Q},\downarrow})$  are coupled leading to the following Green's function matrix [16]

$$G_0^{-1}(z, \mathbf{k}) = \begin{pmatrix} z - \epsilon(\mathbf{k}) & -\Delta(\mathbf{k}) & -i\Phi(\mathbf{k}) & 0 \\ -\Delta(\mathbf{k}) & z + \epsilon(\mathbf{k}) & 0 & i\Phi(\bar{\mathbf{k}}) \\ i\Phi(\mathbf{k}) & 0 & z - \epsilon(\bar{\mathbf{k}}) & -\Delta(\bar{\mathbf{k}}) \\ 0 & -i\Phi(\bar{\mathbf{k}}) & -\Delta(\bar{\mathbf{k}}) & z + \epsilon(\bar{\mathbf{k}}) \end{pmatrix} \quad (1)$$

$\epsilon(\mathbf{k})$  is the one-particle energy,  $\epsilon(\mathbf{k}) = -(\delta t + \alpha J)(\cos(k_x) + \cos(k_y)) - 2t'\delta \cos(k_x)\cos(k_y) - \mu$ , with  $\alpha = 1/N_c \sum_{\mathbf{q}} \cos(q_x) f(\epsilon(\mathbf{q}))$ .  $f$  is the Fermi function,  $\delta$  the doping away from half-filling,  $\mu$  a renormalized chemical potential,  $t$  and  $t'$  are nearest and second-nearest neighbor hopping amplitudes,  $z$  a complex frequency, and  $\bar{\mathbf{k}} = \mathbf{k} - \mathbf{Q}$ .

Expressing the expectation values in the order parameters by  $G_0$  and using Eq.(1) one obtains two coupled equations for the order parameters. In the interesting doping region the order parameters have d-wave symmetry,  $\Phi(\mathbf{k}) = \Phi\gamma(\mathbf{k}), \Delta(\mathbf{k}) = \Delta\gamma(\mathbf{k})$ , with  $\gamma(\mathbf{k}) = (\cos(k_x) - \cos(k_y))/2$ . The equations for  $\Delta$  and  $\Phi$  read then

$$1 = \frac{2(J - V_C)}{N_c} \sum_{\mathbf{k}} \sum_{\alpha=1}^4 \frac{f(E_\alpha(\mathbf{k}))\gamma^2(\mathbf{k})}{\prod_{\beta \neq \alpha} (E_\alpha(\mathbf{k}) - E_\beta(\mathbf{k}))} \left( \gamma^2(\bar{\mathbf{k}})(\Delta^2 + \Phi^2) - (E_\alpha(\mathbf{k}) - \epsilon(\bar{\mathbf{k}}))(E_\alpha(\mathbf{k}) + \epsilon(\bar{\mathbf{k}})) \right), \quad (2)$$

$$1 = \frac{2J}{N_c} \sum_{\mathbf{k}} \sum_{\alpha=1}^4 \frac{f(E_\alpha(\mathbf{k}))\gamma^2(\mathbf{k})}{\prod_{\beta \neq \alpha} (E_\alpha(\mathbf{k}) - E_\beta(\mathbf{k}))} \left( \gamma^2(\bar{\mathbf{k}})(\Delta^2 + \Phi^2) - (E_\alpha(\mathbf{k}) + \epsilon(\mathbf{k}))(E_\alpha(\mathbf{k}) + \epsilon(\bar{\mathbf{k}})) \right). \quad (3)$$

$V_C$  is the expansion coefficient of the Coulomb potential in the d-wave channel with the basis function  $\gamma$ , and  $E_\alpha(\mathbf{k})$  are the four poles of  $G_0(z, \mathbf{k})$  in the  $z$ -plane. At

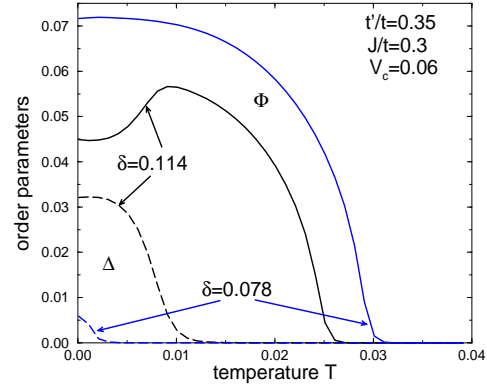


FIG. 1. Order parameters  $\Phi$  and  $\Delta$  as a function of temperature in units of  $t$  for the dopings  $\delta = 0.114$  and  $0.078$ .

zero temperature  $\Phi$  decreases monotonically with increasing  $\delta$ , whereas  $\Delta$  first increases, passes then through a maximum at  $\delta_0$  and finally decreases again, as shown in Fig.1 of Ref. [17]. Fig.1 shows the temperature dependence of  $\Phi$  and  $\Delta$ , calculated with  $t'/t = -0.35$  and  $J/t = 0.3$ . The energy unit is  $t$ . A repulsive nearest-neighbor Coulomb interaction was also included with  $V_C/t = 0.06$ . According to Fig.1 the temperature dependence of the order parameters is mean-field like sufficiently away from  $\delta_0$ . Near  $\delta_0$  the two order parameters strongly interact with each other. For instance, for the slightly underdoped case of  $\delta_0 = 0.114$ , the increase of  $\Delta$  at low temperatures is accompanied by a decrease of  $\Phi$  so that the “total gap”  $\sqrt{\Delta^2 + \Phi^2}$  is rather constant at low temperatures.

Fig.2 contains quasi-particle densities for  $\delta = 0.114$  and  $T = 0$ . The thin dotted line denotes the density for vanishing order parameters. It shows a logarithmic divergence due to the van Hove singularity. The latter lies for the chosen parameters just below the Fermi energy which corresponds to zero energy. The long-dashed curve describes the case where the correct finite value for  $\Phi$  has been used, but  $\Delta$  has been put to zero. This density shows a strongly asymmetric gap structure with a strong peak on the low and a weaker, splitted peak at the high-energy side. A closer analysis shows that the lower peak of this doublet comes from  $\mathbf{k}$ -points near the antinodal points  $X$  and  $Y$ . States near these points are

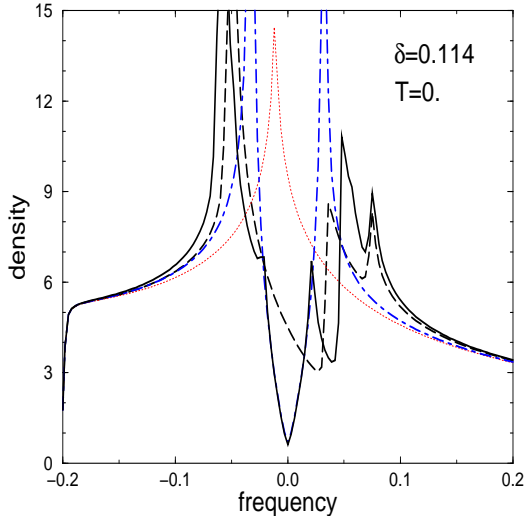


FIG. 2. Density of states for  $\Phi = \Delta = 0$  (thin dotted line),  $\Phi \neq 0, \Delta = 0$  (long-dashed line),  $\Phi = 0, \Delta \neq 0$  (dash-dotted line),  $\Phi \neq 0, \Delta \neq 0$  (solid line) for  $T = 0$  and  $\delta = 0.114$ .

coupled by the d-CDW and their energies are shifted by the formation of the d-wave gap. This explains why this peak moves upwards (see the dashed and solid lines in Fig. 2) in the presence of an additional BCS gap. In contrast to that, the upper peak of the doublet originates from  $\mathbf{k}$ -states on the boundaries of the reduced Brillouin zone near the points  $(\pi/2 - \delta, \pi/2 - \delta)$  and equivalent points with  $\delta \ll \pi/2$ . Their energies are mainly determined by the one-particle energies near this point relative to the Fermi energy and thus less sensitive to the formation of the gap. This explains why the position of this higher peak of the doublet is unchanged by the BCS gap, see the dashed and solid lines in Fig. 2. The density is everywhere nonzero in the d-CDW state, in particular, at the Fermi energy. The asymmetry of the density with respect to zero energy is caused by the asymmetric bare density due to the proximity of the van Hove singularity. The finite density of states at the Fermi energy allows to lower further the ground state energy by introducing a superconducting gap. The density of states becomes then strictly zero at the Fermi level and the additional d-wave gap is rather symmetric with respect to the Fermi energy. The resulting density of states for this case  $\Phi \neq 0, \Delta \neq 0$  is given by the solid line in Fig.2. Comparing this line with the dot-dashed line, which corresponds to a pure SC state  $\Phi = 0, \Delta \neq 0$ , one recognizes that the inner part of the gap structure looks like a reduced SC gap with weakly developed edges, at least on the low-energy side. Fig.3 shows the density of states for  $\delta = 0.114$  and three different temperatures. These temperatures are low enough so that the main gap edges do not change much because  $\sqrt{\Phi^2 + \Delta^2}$  is nearly constant. However, the opening of the SC gap in the inner part of the gap structure can

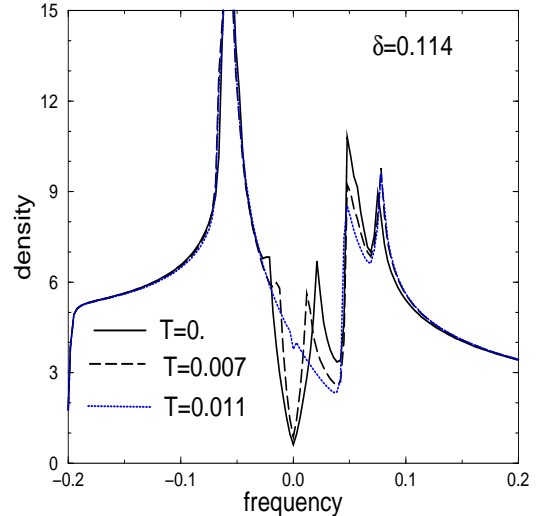


FIG. 3. Density of states for  $T = 0$ . (solid line),  $T = 0.007$  (dashed line),  $T = 0.011$  (dotted line) and  $\delta = 0.114$ .

clearly be seen as a function of temperature.

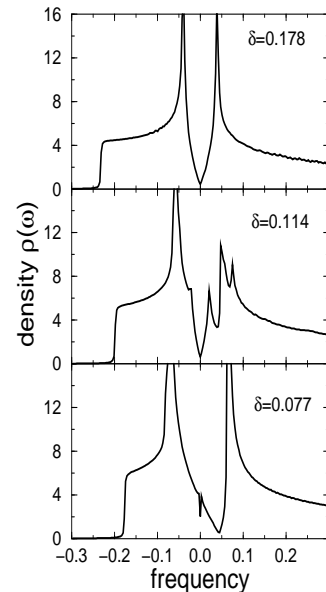


FIG. 4. Density of states for three different dopings at  $T = 0$ .

Figs.2 and 3 illustrate the fact that the total gap is not just one single d-wave gap with an amplitude given by the square root of the sum of the square of the two gaps. Instead, the SC and CDW gaps interact with each other, however in such a way that their individual structures can still be seen in the density of states. This is also apparent in the density plots for three different dopings in Fig.4. The upper and lower panels illustrate the difference between the density of states for a SC and a d

CDW gap, respectively. Some features of the individual gaps are still present in the middle panel of Fig.4 which describes the case of coexisting SC and d CDW gaps. We find in contrast to Ref. [18] that our self-consistently calculated order parameters yield for all considered dopings and hopping parameters densities where the SC gap lies inside the d-CDW gap.

One important feature of the coexisting SC and d-CDW state is that the two gaps have different locations in  $\mathbf{k}$ -space: The CDW gap mainly resides near the  $X$  and  $Y$  points, and the SC gap near the diagonal. This becomes clear by looking at the Fermi lines as a function of  $\Phi$  in the absence of superconductivity. Since a finite  $\Phi$  implies a doubling of the elementary cell we have plotted Fermi

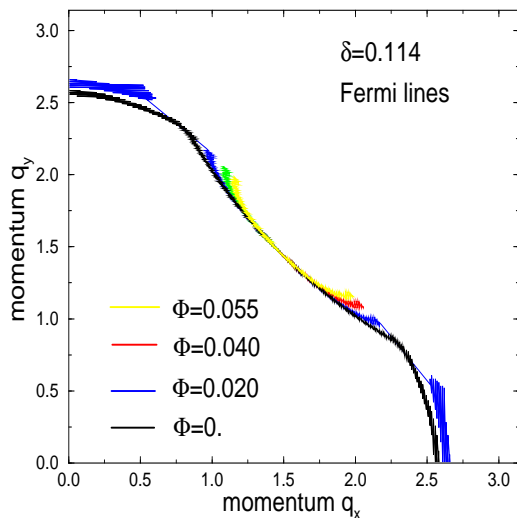


FIG. 5. Fermi lines at  $T = 0$  for four values for  $\Phi$  in the absence of superconductivity.

lines in Fig.5 in the reduced zone scheme, e.g., the new Brillouin zone (BZ) is bounded by a straight line between the points  $X = (\pi, 0)$  and  $Y = (0, \pi)$ . The black line corresponds to  $\Phi = 0$  and describes the usual normal state Fermi line in the reduced Brillouin zone for the parameters  $t'/t = 0.35$  and  $J/t = 0.3$ . For  $\Phi = 0.02$  the Fermi line consists of a long arc around the diagonal ending at the new boundary of the BZ and two pieces near the  $X$  and  $Y$  points. This means that the region around the hot spots becomes first gapped. Increasing  $\Phi$  only the arc around the diagonal survives and becomes shorter. The finite density of states at the Fermi energy in the CDW state is due to this arc. Allowing also for SC the arc becomes gapped and the Fermi line shrinks to one point on the diagonal. The coexistence of SC and CDW thus becomes possible because the CDW state can lower the free energy by introducing a SC gap along the arc.

### III. CONDUCTANCE

Using lowest-order perturbation theory in the inter-layer hopping the quasi-particle c-axis current  $J$  between superconducting layers (SIS junction) is given by [19]

$$J(V) = \frac{e}{\pi} \frac{1}{N_c^3} \sum_{\mathbf{k}, \mathbf{q}, \mathbf{q}'} \ll T_{\mathbf{k}\mathbf{q}} T_{\mathbf{k}'\mathbf{q}'}^* \gg \int_{-\infty}^{\infty} d\omega (f(\omega) - f(\omega + eV)) A_{11}(\mathbf{k}'\mathbf{k}, \omega + eV) A_{11}(\mathbf{q}\mathbf{q}', \omega). \quad (4)$$

In Eq.(4)  $T_{\mathbf{k}\mathbf{q}}$  denotes the hopping matrix element between states with momenta  $\mathbf{k}$  and  $\mathbf{q}$  in adjacent layers and  $\ll \dots \gg$  an average over quenched disorder.  $f$  is the Fermi function,  $V$  the applied voltage, and, using the Nambu representation,  $A_{11}$  the spectral function of the element 11 of the  $2 \times 2$  Green's function matrix. The momenta in the above formula refer to the original (large) BZ. The differential conductance  $G(V)$ , which is the main quantity of interest in the following, is defined as the first derivative of  $J$  with respect to  $V$ .

We make the following Ansatz for the averaged squared tunneling matrix element

$$\ll T_{\mathbf{k}\mathbf{q}} T_{\mathbf{k}'\mathbf{q}'}^* \gg = t_{\perp}^2 \gamma(\mathbf{k}) \gamma(\mathbf{q}) \gamma(\mathbf{k}') \gamma(\mathbf{q}') N_c \delta_{\mathbf{k}-\mathbf{q}, \mathbf{k}'-\mathbf{q}'} (a \delta_{\mathbf{k}, \mathbf{q}} + g(\mathbf{k} - \mathbf{q})). \quad (5)$$

The form factors  $\gamma(\mathbf{k})$  determine which electrons in the BZ are mainly involved in the tunneling process. Results from band structure calculations [20] suggest the Ansatz [21]

$$\gamma(\mathbf{k}) = 1 - u + u/2 |\cos k_x - \cos k_y|, \quad (6)$$

with  $0 \leq u \leq 1$ . The parameter  $u$  interpolates between the isotropic case  $u = 0$  and the strongly anisotropic case  $u = 1$ . The latter is typical for tunneling within a double layer of  $\text{CuO}_2$  planes, whereas tunneling between layers in different elementary cells may include also an isotropic component. The first term in the brackets in Eq.(5) accounts for coherent scattering with strength  $a$ . The second term in the brackets describes incoherent scattering where  $g$  is a smooth function of the momentum. One may distinguish two cases for the momentum dependence of  $g$ . In the case of strong, localized scatterer  $g$  may assumed to be completely independent on momentum. If long-ranged random fields are present  $g$  is large (small) mainly at small (large) momentum transfers. The momentum dependence of  $g$  thus can be modelled by

$$g(\mathbf{k}) = g \cdot \exp(-|\mathbf{k}|^2/\Lambda^2), \quad (7)$$

where the momentum  $\Lambda$  interpolates from isotropic to forward scattering, described by large and small values for  $\Lambda$ , respectively.

Since the case of coherent scattering can be obtained from that of incoherent scattering by replacing  $g$  by  $4\pi/\Lambda^2$  and taking the limit  $\Lambda \rightarrow 0$  we will first consider

incoherent scattering. Using Eq.(5) and restricting the momenta to the reduced BZ because of the cell doubling due to the d-CDW we obtain for the tunnel current

$$J(V) = \frac{e}{\pi} \frac{t_{\perp}^2}{N_c^2} \sum_{\tilde{\mathbf{k}}\tilde{\mathbf{q}}} \gamma^2(\tilde{\mathbf{k}})\gamma^2(\tilde{\mathbf{q}}) \int_{-\infty}^{\infty} d\omega (f(\omega) - f(\omega + eV))$$

$$\left( g(\tilde{\mathbf{k}} - \tilde{\mathbf{q}}) \sum_{ii'=0,1} A_{1+2i,1+2i'}(\tilde{\mathbf{k}}, \omega + eV) A_{1+2i',1+2i}(\tilde{\mathbf{q}}, \omega) \right.$$

$$+ g(\tilde{\mathbf{k}} - \tilde{\mathbf{q}} - \mathbf{Q})(A_{11}(\tilde{\mathbf{k}}, \omega + eV) A_{33}(\tilde{\mathbf{q}}, \omega)$$

$$+ A_{33}(\tilde{\mathbf{k}}, \omega + eV) A_{11}(\tilde{\mathbf{q}}, \omega) \left. \right). \quad (8)$$

The tilde on the momenta indicates that these momenta lie in the reduced BZ. The spectral functions  $A_{ij}$  can be assumed to be periodic with respect to the reduced BZ. The same is true for the form factors  $\gamma$  but not for the function  $g$  which originates from impurity potentials. To make the expression for  $J(V)$  independent of the choice for the reduced BZ we also translate back the momentum appearing in  $g$  to the reduced BZ. Eq.(8) then becomes

$$J(V) = \frac{e}{\pi} \frac{t_{\perp}^2}{N_c^2} \sum_{\tilde{\mathbf{k}}\tilde{\mathbf{q}}} \gamma^2(\tilde{\mathbf{k}})\gamma^2(\tilde{\mathbf{q}}) \int_{-\infty}^{\infty} d\omega (f(\omega) - f(\omega + eV))$$

$$g(\tilde{\mathbf{k}} - \tilde{\mathbf{q}}) \left( (A_{11}(\tilde{\mathbf{k}}, \omega + eV) + A_{33}(\tilde{\mathbf{k}}, \omega + eV))(A_{11}(\tilde{\mathbf{q}}, \omega) \right.$$

$$+ A_{33}(\tilde{\mathbf{q}}, \omega)) + 2A_{13}(\tilde{\mathbf{k}}, \omega + eV) A_{31}(\tilde{\mathbf{q}}, \omega) \left. \right). \quad (9)$$

The first contribution in the big parantheses describes s-wave, the second one d-wave scattering. Their relative importance is controlled by the parameter  $p_c$  in the function  $g$ . If  $g$  is independent of the transferred momentum Eq.(8) simplifies to

$$J(V) = \frac{egt_{\perp}^2}{\pi} \int_{-\infty}^{\infty} d\omega (f(\omega) - f(\omega + eV)) \tilde{\rho}(\omega + eV) \tilde{\rho}(\omega), \quad (10)$$

with the weighted density

$$\tilde{\rho}(\omega) = \frac{1}{N_c} \sum_{\tilde{\mathbf{k}}} \gamma^2(\tilde{\mathbf{k}}) (A_{11}(\tilde{\mathbf{k}}, \omega) + A_{33}(\tilde{\mathbf{k}}, \omega)). \quad (11)$$

For a SIN junction one usually assumes that  $g$  is independent of momentum. Its current is then obtained from Eq.(10) by identifying one of the two densities with that of the normal metal  $\tilde{\rho}_M$  which can be assumed to be constant. The resulting conductance of a SIN junction becomes then at not too high temperatures

$$G_{SIN}(V) = \frac{eg\tilde{\rho}_M}{\pi} \tilde{\rho}(eV). \quad (12)$$

Since we will mainly consider SIS junctions in the following conductance will always refer to SIS junctions unless it is stated otherwise.

The simplest case of incoherent scattering corresponds to  $u = 0$  and  $\Lambda = \infty$ , i.e., where the averaged tunneling matrix element is independent of all momenta. Using the densities of Fig.4 the resulting conductance curves are shown in Fig.6. In the pure superconducting state (upper panel) the conductance shows a broad peak near the gap  $2\Delta$  which decays rapidly towards larger but rather slow towards smaller energies. The conductance is positive for all frequencies, especially also above  $2\Delta$ , which is intimately connected to the presence of the large and rather constant density of states outside of the gap region. In the d-CDW case (lower panel in Fig.6) the conductance curve has two peaks. The higher and dominant one is due to the CDW gap  $2\Phi$ . In contrast to the superconductor the d-CDW state has (neglecting the tiny BCS-gap at the doping  $\delta = 0.077$ ) a finite density of

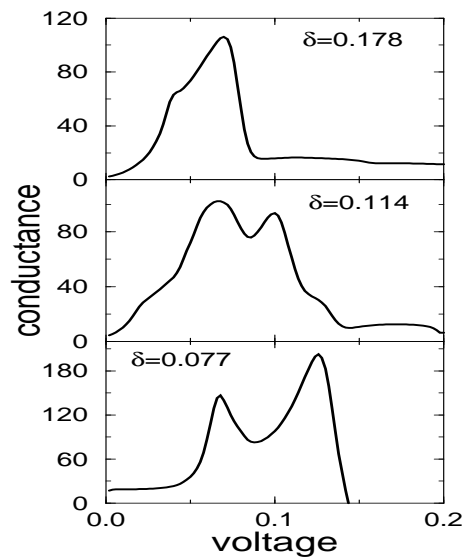


FIG. 6. Incoherent c-axis conductance calculated for  $u=0$ ,  $\Lambda = \infty$ ,  $T=0$ ,  $J=0.3$ ,  $t'=-0.35$ , and three different dopings.

states at and near the Fermi energy along the arcs. The folding of these states with one of the CDW edges causes the lower peak at about the energy  $\Phi$ . Well above  $2\Phi$  the curve is again rather constant and partly slightly negative. In the weakly underdoped case (middle panel in Fig.6) the conductance curve shows essentially two peaks. They arise due to the folding of the large CDW shoulder at negative frequencies with the BCS peak and the two splitted CDW shoulders at positive frequencies, respectively. The BCS gap itself is seen only as a broad and weak structure at low energies. Some of the features in Fig.6 agree with the tunneling experiments, e.g., the monotonic increase of the dominant high-frequency peak with decreasing doping and the appearance of more than one peak in the optimally and underdoped cases. However, several details of these curves are not found in the experiments: The peak in the overdoped case is much too

broad compared to that in the intrinsic c-axis tunneling spectra of Ref. [6], the lower peak in the underdoped cases is caused by the relaxation of electronic states around the CDW gap to states near the arcs or the nearby BCS gap and thus does not approach zero at  $T_c$  as in intrinsic tunneling spectra. Similar conclusions are reached, following Eq.(12), by comparing the experimental conductance curves of *SIN* junctions [3,4] with the densities of Fig.4. The monotonic increase of the distance between the two main peaks with decreasing doping occurs in both cases but the experiment does not show the asymmetry of the theoretical conductance curve in the underdoped case as well as the additional structures obtained in the region of coexisting SC and d CDW.

Things change substantially if the form factor  $\gamma(\mathbf{k})$  with a non-zero value for  $u$  is taken into account. Assuming still a momentum-independent function  $g$  the tunnel current is now to be calculated from the weighted density  $\tilde{\rho}$  as given by Eqs.(10) and (11). Fig.7 shows  $\tilde{\rho}(\omega)$  for

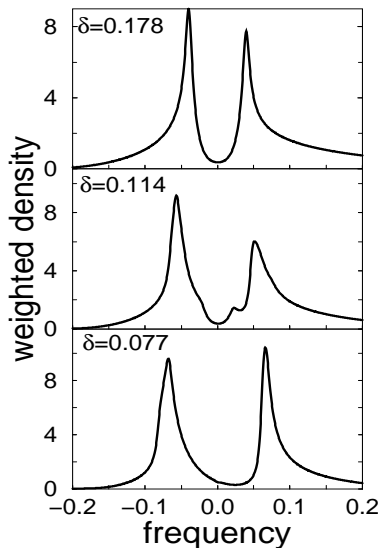


FIG. 7. Weighted density  $\tilde{\rho}$  as a function of frequency for  $T=0$ ,  $J=0.3$ ,  $\eta = 0.004$ ,  $t'=-0.35$ , and three different dopings  $\delta$ .

the extreme anisotropic case  $u = 1$  for three different dopings. Most of the background contribution to the density has been removed. In the over- and under-doped cases (upper and lower panels in Fig. 7)  $\tilde{\rho}$  consists of just two rather symmetric peaks with respect to  $\omega = 0$  which are related to the superconducting and d-CDW gaps, respectively. In the slightly underdoped regime, where SC and d-CDW coexist,  $\tilde{\rho}$  is still rather symmetric with respect to  $\omega = 0$  and consists of four peaks. The peaks at large energies are dominant, their frequencies are roughly given by  $\pm 2\sqrt{\Phi^2 + \Delta^2}$ , i.e., they describe the “total” gap of the two components. The two weaker and less pro-

nounced peaks at smaller frequencies are related to the SC gap, which can be concluded from their temperature dependence and magnitude of their energies. The low intensities of these peaks can also be easily understood: The BCS gap resides on the arcs near the diagonal. The form factor  $\gamma$  with  $u = 1$  suppresses heavily the tunneling of states in this region. It is also interesting to note that only the lower peak of the splitted high-energy d-CDW edge in Fig.4 for  $\delta = 0.114$  survives in the corresponding weighted density in Fig.7. This can easily be understood by noting that the lower (higher) peak of the doublet is due to  $\mathbf{k}$ -states near the antinodal (nodal) points and thus unaffected (suppressed) by the form factor.

The curves for  $\tilde{\rho}$  look in many respects similar to the experimental *SIN* conductance curves. In both cases, the spectra are dominated by two pronounced peaks lying rather symmetrically with respect to  $\omega = 0$  and whose separation increases monotonically with decreasing doping. These peaks evolve in  $\tilde{\rho}$  very smoothly from a SC to a d CDW state passing through a region where both order parameters coexist. The agreement can be further improved if one introduces a phenomenological damping in the theoretical curves. The peaks are then broadened

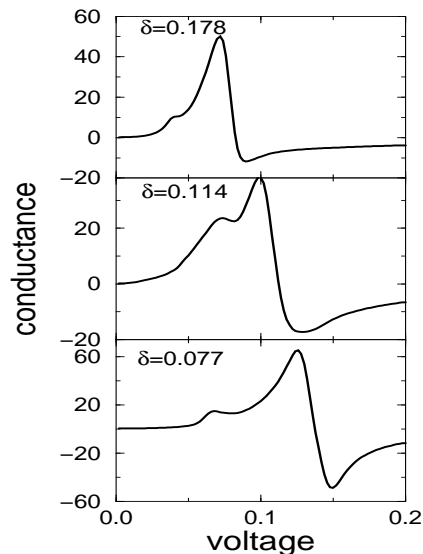


FIG. 8. Incoherent c-axis conductance calculated for  $u=1$ ,  $\Lambda = \infty$ ,  $T=0$ ,  $t'=-0.35$ , and three different dopings.

and the low-energy structures for  $\delta = 0.114$  become invisible. The dip on the high-energy sides of the main peaks in the experimental spectra is, however, missing in  $\tilde{\rho}$  indicating the presence of self-energy effects beyond a constant damping.

Performing the frequency integral in Eq.(10) with the weighted densities  $\tilde{\rho}$  one obtains the curves of Fig.8. The main effect of the inclusion of the anisotropic form factors  $\gamma$  with  $u = 1$  is the suppression of the small quasi-

particle excitations near the nodal regions. This means in the overdoped case  $\delta = 0.178$  that the slowly decaying tail of the main peak towards lower voltages seen in the upper panel of Fig.6 is substantially suppressed making the peak much sharper. The dip above  $2\Delta$  is also more pronounced than in Fig.6 and the conductance assumes (small) negative values over a wide region towards higher voltages. The reason for this negative resistance becomes clear from a comparison of Figs.4 and 7. Most of the rather constant background density in Fig.4 has been removed by the anisotropic form factor. However, just this constant background density is responsible for a positive and structureless conductance outside of the gap region. Similar considerations apply to the underdoped case  $\delta = 0.077$ . The anisotropic form factor sharpens up somewhat the high voltage peak and suppresses the lower peak at around  $\Phi$  because the states near the arcs can no longer contribute much. At the same time the conductance shows a well-pronounced dip above  $2\Phi$  with large negative values due to the eliminated background density of states. Similar statements hold for the slightly underdoped case. Here the lower peak at around  $\Delta + \Phi$ , which was in Fig. 6 still the strongest one, is suppressed but still visible.

The above calculations show that an incoherent tunneling model with a momentum independent function  $g$  is not able to produce a peak in the coexistence region which moves towards zero voltage if  $T$  approaches  $T_c$ .

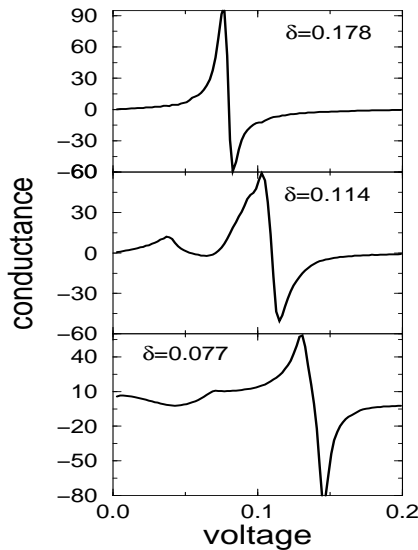


FIG. 9. Incoherent c-axis conductance calculated for isotropic  $u = 0$  form factors, a momentum cutoff  $\Lambda = \pi/8$ ,  $T = 0$ ,  $J = 0.3$ ,  $t' = -0.35$  and three different dopings  $\delta$ .

We therefore have also studied finite values for  $\Lambda$  in the Gaussian in Eq.(7). Experimental evidence for strong forward scattering in the averaged squared tunneling matrix element has recently been found from the temperature dependence of the c-axis penetration depth in

$YBa_2Cu_3O_{+x}$  [22]. Using the isotropic form factor  $u = 0$  and  $\Lambda = \pi/8$  Fig.9 shows the conductance for three different dopings at  $T=0$ . The spectra are dominated by a peak at approximately the frequencies  $2\sqrt{\Phi^2 + \Delta^2}$ . This peak reflects the doping dependence of the “total” gap which increases monotonically with decreasing doping. In the upper panel the gap describes a superconducting gap, in the lower panel a d-CDW gap and in the middle panel a combination of both. The doping dependence of the main peak in Fig.9 agrees well with experimental SIS spectra, see, for instance, Figs. 1 and 2 in [5], though the dips above the main line are more pronounced than in the experiment. Also negative conductances are only very rarely observed experimentally. In the slightly underdoped regime (middle panel in Fig.9) the two order parameters coexist. The conductance shows in this case besides of the dominating high-frequency peaks a peak near the superconducting part of the gap. This peak moves towards smaller frequencies with increasing temperature and vanishes at  $T_c$ . The exact energy position of this peak is somewhat below the superconducting part of the gap,  $2\Delta$ . This can easily be understood from Figs.2 and 3: Due to the interaction between the two gaps part of the BCS shoulder has been removed by the d-CDW so that the superconducting part of the gap appears smaller than the canonical value for  $2\Delta$ . This reduced gap

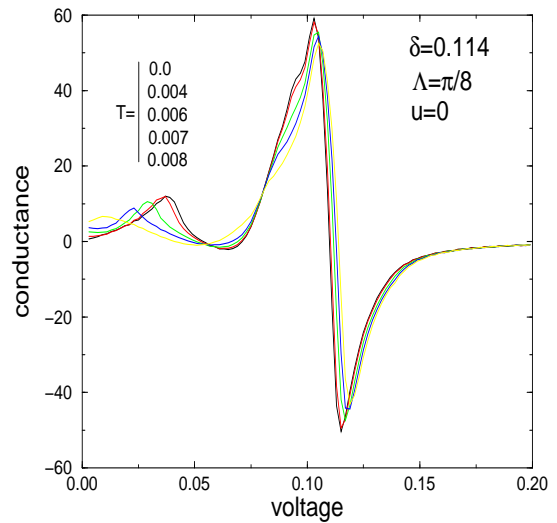


FIG. 10. Incoherent c-axis conductance for five temperatures using a Gaussian distributed hopping matrix element with width  $\Lambda = \pi/8$ . Increasing temperatures correspond to curves with energetically decreasing low-energy peaks.

exhibits the expected temperature dependence as can be seen from Fig.3. The upper and lower panels in Fig.9 also show weak structures at low voltages. A closer inspection, however, reveals that these structures are caused by the underlying band structure and are unrelated to the BCS gap. The spectra in Fig.9 exhibit well-pronounced

dips at energies somewhat above the main peaks. These dips, which are also seen in tunneling spectra from break junctions, have been associated with self-energy effects due to the coupling to some boson [2,5]. We would like to stress that no self-energy effects have been taken into account in calculating Fig.9. Simple model calculations indicate that one finds easily a dip in SIS spectra if the size of the region above  $2\Delta$  where spectral weight piles up because of the formation of the gap is comparable or smaller than the gap.

Fig.10 shows the temperature dependence of the incoherent conductance for  $\delta = 0.114$  and  $\Lambda = \pi/8$ . The dominating higher peak is practically temperature independent for the temperatures shown in the figure. On the other hand, Fig.1 indicates that both order parameters vary in the considered temperature interval. One concludes from this that the higher peak reflects the total gap which is rather independent of temperature. In contrast to that, the lower peak depends strongly on temperature. It moves towards zero frequency with increasing temperature, loses spectral weight and vanishes with vanishing  $\Delta$ . Intrinsic c-axis tunneling spectra in various cuprates show essentially the same features as in Fig. 10. In particular, the observed low-frequency peak, which

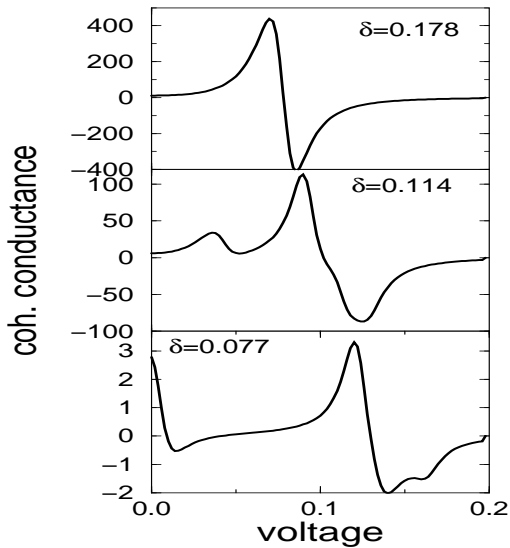


FIG. 11. Coherent c-axis conductance for anisotropic  $u=1$  form factors,  $T=0$ ,  $J=0.3$ ,  $t'=-0.35$ ,  $\eta = 0.01$ , and three different dopings  $\delta$ .

seems not to be affected much by heating effects, also moves towards zero frequency with increasing temperature and vanishes near  $T_c$ . We would like to point out that this BCS-like peak can be seen in incoherent scattering only for a rather isotropic form factor  $\gamma$ . Otherwise, the tunneling of electrons near the nodal direction, where the SC gap is located, is too much suppressed. Another prerequisite is that the averaged tunneling matrix element must be strongly momentum-dependent causing

strong forward scattering.

Besides of incoherent tunneling the quasiparticle current always contains a contribution  $J_{coh}$  due to coherent tunneling, originating from the first term in the parentheses in Eq.(5).  $J_{coh}$  is given by Eq.(4) with  $g$  replaced by  $a\delta_{\mathbf{k},\mathbf{q}}$ . The explicit expression for  $J_{coh}$  thus becomes

$$J_{coh}(V) = \frac{eat_{\perp}^2}{\pi} \frac{1}{N_c} \sum_{\tilde{\mathbf{k}}} \gamma^4(\tilde{\mathbf{k}}) \int_{-\infty}^{\infty} d\omega (f(\omega) - f(\omega + eV)) \sum_{ii'=0,1} A_{1+2i,1+2i'}(\tilde{\mathbf{k}}, \omega + eV) A_{1+2i',1+2i}(\tilde{\mathbf{k}}, \omega). \quad (13)$$

If the superconducting order parameter is zero, Eq.(1) reduces to a  $2 \times 2$  matrix. Calculating explicitly the spectral functions from this matrix and performing the frequency integration in the above integral one finds then that the sum over  $i, i'$  yields zero without any further approximation. One thus obtains the important result that coherent tunneling is zero in a pure d-CDW.

Fig.11 shows the coherent conductance for  $u = 1$ ,  $T = 0$ , and three different dopings. The spectral functions were obtained from the Green's functions using the frequency  $\omega + i\eta$  with  $\eta = 0.01$ . In the overdoped and slightly underdoped case the curves are similar to those in Fig.9. In particular, corresponding curves have negative conductances above the main peak caused by the restriction to small momentum transfers in the tunneling process. For  $\delta = 0.114$  both curves show besides of the main peak associated with the total gap a second peak at smaller energies with BCS properties. However, one should note that Fig.9 was calculated with  $u = 0$  whereas Fig.11 with  $u = 1$ . It is somewhat surprising that coherent tunneling shows still the BCS peak though most electrons near the nodal direction are prevented from tunneling due to the employed strongly anisotropic form factor. The dominance of small energy features in coherent tunneling also is present in the underdoped case  $\delta = 0.077$  where the tiny BCS gap causes a sharp structure at very low energies. One important feature in Fig.11 is related to the absolute values for the conductance depicted along the y-axis. The coherent conductance drops dramatically with decreasing doping. Going to smaller doping values one finds that  $J_{coh}$  becomes zero if the superconducting order parameter vanishes in agreement with the above analytic result. Coherent tunneling is non-zero in case of a pure superconductor as shown by the upper panel in Fig. 11. However, it is zero for a pure d-CDW state and the d-CDW gap can only be probed in the presence of superconductivity. If the identification of the pseudogap phase with a d-CDW is correct coherent tunneling should vanish in the pseudogap phase.

Fig.12 illustrates the dependence of the coherent conductance on temperature for  $\delta = 0.114$ . With increasing temperature the position of the low-energy peak and its intensity decrease and approach zero at around



$T = 0.0081$  where the superconducting order parameter vanishes. The position of the high-energy peak as well

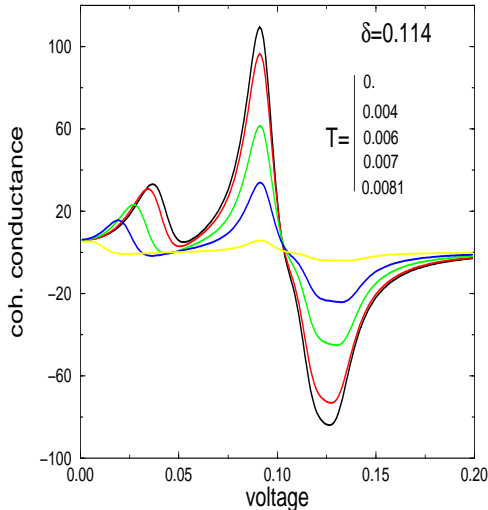


FIG. 12. Coherent c-axis conductance for anisotropic  $u=1$  form factors,  $J=0.3$ ,  $t'=-0.35$ ,  $\eta = 0.01$ , and various temperatures labeled according to decreasing maxima.

as the dip are rather independent of temperature but the intensity of the whole high-energy part drops dramatically with temperature and vanishes at  $T = 0.0081$ . This again demonstrates that contributions from the d-CDW can only be seen in the conductance if the superconducting order parameter is finite, i.e., in the coexistence regime.

#### IV. SELF-ENERGY EFFECTS

According to angle-resolved photoemission experiments the generic spectral function in the superconducting state consists of a well pronounced peak followed by a dip and a hump towards larger energies [1]. In concordance with that the electron dispersion shows a kink between 30 and 70 meV below the Fermi energy [23]. These features occur throughout the underdoped, optimally doped and the overdoped regime. Most of these properties can be reproduced in a model where the electrons interact with a boson branch (which may be a phonon or a spin fluctuation) [24–26]. In the following we assume a dispersionless boson branch with a constant dimensionless coupling  $\lambda$ . In the presence of SC and d CDW the inverse of the electronic  $4 \times 4$  Green's function  $G(z, \mathbf{k})$  satisfies

$$G^{-1}(z, \mathbf{k}) = G_0^{-1}(z, \mathbf{k}) - \Sigma(z, \mathbf{k}), \quad (14)$$

where  $G_0^{-1}$  is given by Eq.(1) and  $\Sigma$  is the self-energy. Because the boson-mediated interaction is momentum-

independent in our model  $\Sigma$  has only diagonal elements and it is  $\Sigma_{11} = \Sigma_{22} = \Sigma_{33} = \Sigma_{44}$ , with

$$\Sigma_{11}(z) = -\frac{g^2}{N_c} \sum_{\tilde{\mathbf{k}}} \left( \sum_{\alpha=1}^4 \frac{2\omega_0 s(E_\alpha) f(E_\alpha)}{((z - E_\alpha)^2 - \omega_0^2) \prod_{\beta \neq \alpha} (E_\alpha - E_\beta)} + \frac{b(-\omega_0) s(z - \omega_0)}{\prod_{\alpha} (z - \omega_0 - E_\alpha)} - \frac{b(\omega_0) s(z + \omega_0)}{\prod_{\alpha} (z + \omega_0 - E_\alpha)} \right). \quad (15)$$

$g^2$  is related to  $\lambda$  by  $g^2 = \lambda \omega_0 / (2N(0))$ , where  $N(0)$  is the density of states for one spin direction and  $\omega_0$  the frequency of the boson.  $E_\alpha$  denote the four poles of  $G^{(0)}$ ,  $b$  the Bose function, and  $N_c$  is two times the number of allowed momenta  $\tilde{\mathbf{k}}$ .  $s(z)$  is given by

$$s(z) = 2z(z^2 - (\epsilon^2(\mathbf{k}) + \epsilon^2(\mathbf{k} - \mathbf{Q}))/2 - \Delta^2(\mathbf{k}) - \Phi^2(\mathbf{k})). \quad (16)$$

Fig. 13 shows the real and imaginary parts of the retarded self-energy  $\Sigma_{11}(\omega + i\eta)$  at  $T = 0$ . The curves for different dopings look rather similar. The gap near the Fermi energy consists of the phonon energy plus the d-wave gap of the SC and/or d-CDW state. The panels in the figure illustrate the very smooth transition from a SC to a d-CDW gap with decreasing doping, passing also very smoothly through the coexistence region of SC and d-CDW. We used in this and in all the following figures

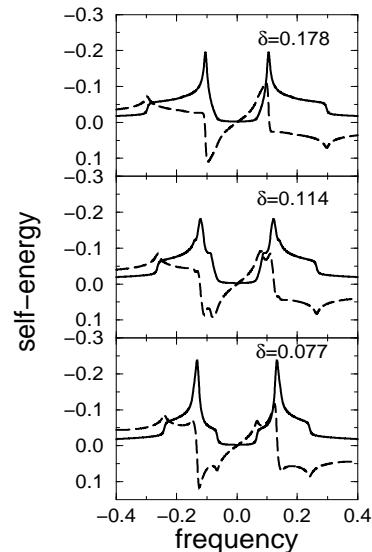


FIG. 13. Real (dotted line) and imaginary (solid line) parts of the self-energy for  $T=0$ ,  $\omega_0 = 0.065$ ,  $\eta = 0.004$ , and  $\lambda = 1$ .

the value 1 for the dimensionless coupling constant  $\lambda$ . This value corresponds to a change of the slope of the electron dispersion at the kink by a factor two in rough agreement with the photoemission data.

Fig.14 shows the SIN conductance using the  $u = 1$  anisotropic hopping form factor and including self-energy effects. It is instructive to compare this figure with the

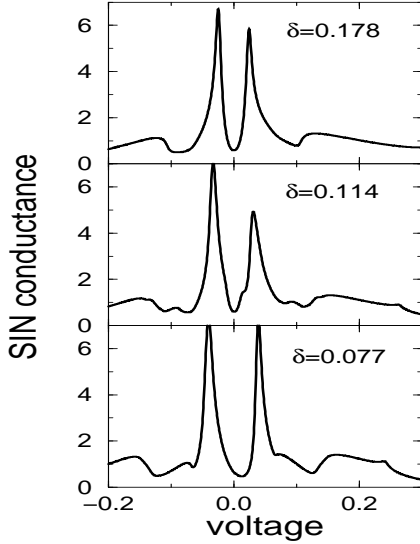


FIG. 14. SIN conductances with self-energy corrections for  $T=0$ ,  $u=1$ ,  $\omega_0 = 0.065$ ,  $\eta = 0.004$ ,  $\lambda = 1$ , and three dopings.

analogous Fig.7 where self-energy effects have been omitted. The BCS-structure seen in Fig.7 for  $\delta = 0.114$  has practically vanished in Fig.14. The peaks in Fig.14 are slightly broader, but the main effect of the self-energy is to move spectral weight from the main peaks to the sidebands. In the pure superconducting state at  $\delta = 0.178$  the sidebands consists of a clear dip and hump whereas in the two other cases the dip-hump feature is less pronounced. Both dip and hump move monotonically towards larger voltages with decreasing doping. The position of the dip in a pure superconductor is approximately half of the gap plus the boson energy. This rule also holds in the d-CDW and the mixed states. The exact differences between the main peaks and the dip, however, fluctuate between 0.065 and 0.087 in Fig.14. Though the dip in the SIN spectra is solely caused by the interaction with the bosons it may thus be difficult to determine precisely the boson energy from it.

The solid and dashed lines in Fig.15 are conductance curves for incoherent tunneling with and without self-energy effects, respectively. The bosons do not contribute to the non-diagonal self-energy because of the assumed momentum-independent coupling to the electrons. As a result, the bosons diminish both the SC and the d-CDW gaps via their diagonal self-energies. Consequently, the main peak moves towards lower frequencies but, considered as a function of doping, this peak increases monotonically with decreasing doping as in the case without self-energy. Fig.15 also illustrates that the distance between the dip and the main peak is similar in the curves with and without self-energy effects and thus is rather unrelated with the boson energy. For instance, at  $\delta = 0.178$  the distance between the dip and the main peak is 0.020 and 0.018 in the case with and without self-energy, re-

spectively, and thus much smaller than the boson energy of 0.065.

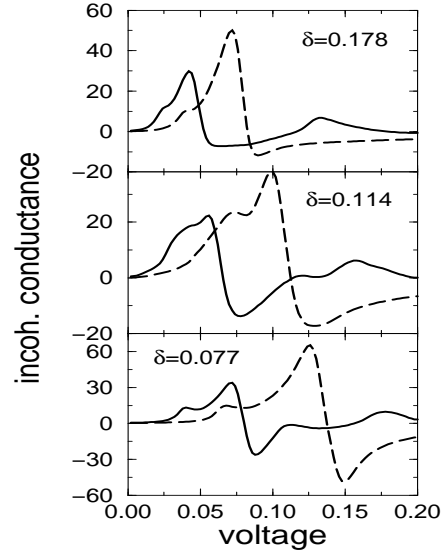


FIG. 15. Incoherent conductances with (solid line) and without (dashed line) self-energy corrections for  $T=0$ ,  $u=1$ ,  $\Lambda = \infty$ ,  $\omega_0 = 0.065$ ,  $\eta = 0.004$ ,  $\lambda = 1$ , and three dopings.

If the experimental SIS spectra correspond to incoherent tunneling the boson energy cannot be obtained from the distance between the main peak and dip. Since the incoherent SIS spectrum is the folding of the SIN spectrum in energy the incoherent SIS spectrum could have, in principle, a dip when the lower main peak is multiplied by the dip at positive voltages and this dip position would be equal to the full gap plus the boson energy. The upper panel of Fig.15, however, shows that the folding in energy does not lead to a dip just below the maximum of the sideband. The main effect of the self-energy in Fig.15 is to shift spectral weight from the main peak to the sideband consisting of a broad hump which monotonically moves towards larger voltages with decreasing doping. This hump is due to the folding of the (occupied) lower main peak with the (unoccupied) upper sidebands in Fig.14. The solid and dashed lines in Fig.16 represent coherent conductance curves with and without self-energy effects, respectively. We have omitted curves for the strongly underdoped case  $\delta = 0.077$  because they are smaller by two order of magnitudes due to the smallness of the superconducting order parameter in this case. Self-energy effects shift the main peaks to smaller energies, diminish somewhat the regions of negative conductance, and create weak sidebands. Figs.7 and 14-16 suggest that self-energy effects and thus the nature of the boson spectrum appear more clear-cut in the SIN than in the SIS spectra. For instance, the dip in the SIN spectrum is solely caused by self-energy effects whereas that in the SIS spectrum is present even in the absence of any self-energy. The curves for the purely su-

perconducting case in Figs.14 and 15 are similar to those published in Refs. [24,27].

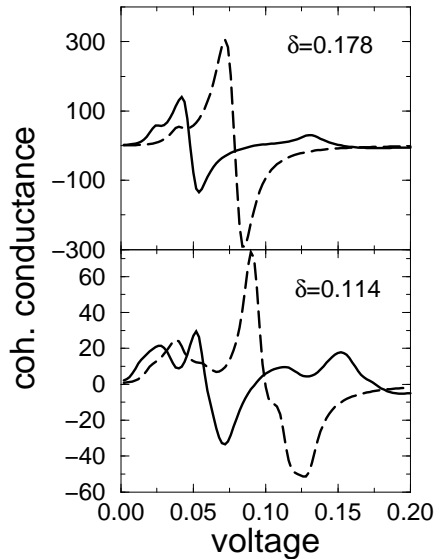


FIG. 16. Coherent conductances with (solid line) and without (dashed line) self-energy corrections for  $T=0$ ,  $u=1$ ,  $\omega_0 = 0.065$ ,  $\eta = 0.004$ ,  $\lambda = 1$ , and two dopings.

## V. CONCLUSIONS

The  $t-J$  model exhibits in the employed large- $N$  limit a d-CDW phase at lower dopings besides of the superconducting phase which is a natural candidate for the pseudogap phase observed in the cuprates. The density of states in the pure d-CDW state is strongly reduced near the Fermi level but still everywhere finite. This means that only part of the Fermi lines of the normal state are destroyed by the d-CDW and that the remaining Fermi lines form arcs around the nodal direction ending at the boundaries of the reduced Brillouin zone. With decreasing doping the length of the arcs become shorter. The ground state energy of the d-CDW can be lowered by introducing a d-wave superconducting gap near the arcs which explains the occurrence of a coexistence region of SC and d-CDW. Because the two gaps are well separated in  $\mathbf{k}$ -space (the d-CDW gap resides near the antinodal, the superconducting gap near the nodal direction) features of the individual gaps survive even in the coexistence regime.

In order to test the applicability of the above picture to cuprates we have calculated coherent and incoherent conductances and compared them with experimental spectra from break-junctions and intrinsic tunneling spectroscopy. We find good evidence that the tunneling matrix element between layers is strongly anisotropic, suppressing tunneling of electrons near the nodal direction,

which is in agreement with band structure arguments. Incoherent tunneling thus probes mainly electrons near the maximal gap at the X and Y points. This gap transforms in a very smooth way from a superconducting gap at large dopings to a d-CDW gap at small dopings passing continuously through the coexistence regime. Calculated incoherent conductances thus fit best to the observed spectra from break-junctions which are characterized by one peak moving monotonically to larger voltages with decreasing doping. We find that coherent tunneling is only non-zero for a non-vanishing superconducting order parameter. Below  $T_c$  it shows in spite of the anisotropic tunneling matrix element two peaks which can be associated with SC and d-CDW. The appearance of a low-energy peak in the calculated coherent tunneling spectrum, which moves to 0 if  $T_c$  is approached from below, is unique for intrinsic tunneling spectra. From this we conclude that tunneling in stacked, intrinsic junctions is dominated by coherent tunneling and that the appearance of the low-energy peak related to superconductivity supports models with two competing order parameters in the underdoped region. Including self-energy effects due to the coupling of electrons to a dispersionless boson branch as suggested by ARPES removes part of the regions of negative resistances and also creates sidebands which, at least in the case of SIN junctions, resemble those which have been measured.

The authors thank Secyt and the BMBF ( Project ARG 99/007) for financial support and A. Yurgens and V.M. Krasnov for useful discussions.

- 
- [1] A. Damascelli, Z.-X. Shen, and Z. Hussain, *Rev. of Mod. Physics* **75**, 473 (2003)
  - [2] Y. DeWilde, N. Miyakawa, P. Guptasarma, M. Iavarone, L. Ozyuzer, J.F. Zasadzinski, P. Romano, D.G. Hinks, C. Kendziora, G.W. Crabtree, and K.E. Gray, *Phys. Rev. Lett.* **80**, 153 (1997)
  - [3] Ch. Renner, B. Revaz, J.Y. Genoud, K. Kadowaki, and Ø. Fischer, *Phys. Rev. Lett.* **80**, 149 (1998)
  - [4] N. Miyakawa, J.F. Zasadzinski, L. Ozyuzer, P. Guptasarma, D.G. Hinks, C. Kendziora, and K.E. Gray, *Phys. Rev. Lett.* **83**, 1018 (1999)
  - [5] J.F. Zasadzinski, L. Ozyuzer, N. Miyakawa, K.E. Gray, D.G. Hinks, and C. Kendziora, *Phys. Rev. Lett.* **87**, 067005 (2001)
  - [6] M. Suzuki, T. Watanabe, and A. Matsuda, *Phys. Rev. Lett.* **82**, 5361 (1999)
  - [7] A. Yurgens, D. Winkler, T. Claeson, S.-Ju Hwang, and Jin-Ho Choy, *Int. J. Mod. Phys. B* **13**, 3758 (1999)
  - [8] V.M. Krasnov, A. Yurgens, D. Winkler, P. Delsing, and T. Claeson, *Phys. Rev. Lett.* **84**, 5860 (2000)
  - [9] M. Suzuki and T. Watanabe, *Phys. Rev. Lett.* **85**, 4787 (2000)

- [10] V.M. Krasnov, A.E. Kovalev, A. Yurgens, and D. Winkler, Phys. Rev. Lett. **86**, 2657 (2001)
- [11] V.M. Krasnov, cond-mat/0201287 (2002)
- [12] A. Yurgens, D. Winkler, T. Claeson, S. Ono, and Y. Ando, Phys. Ref. Lett. **90**, 147005-1 (2003)
- [13] V.M. Krasnov, cond-mat/0308080 (2003)
- [14] V.N. Zavaritsky, cond-mat/0306081
- [15] A. Yurgens, D. Winkler, T. Claeson, S. Ono, and Y. Ando, cond-mat/0309131
- [16] E. Cappelluti and R. Zeyher, Phys. Rev. B **59**, 6475 (1999)
- [17] R. Zeyher and A. Greco, Phys. Rev. Lett. **89**, 177004 (2002)
- [18] W. Kim, J.X. Zhu, J.P. Carbotte, and C.S. Ting, cond-mat/0106594
- [19] J.R. Schrieffer, D.J. Scalapino, and J.W. Wilkins, Phys. Rev. Lett. **10**, 336 (1963)
- [20] O.K. Andersen, A.I. Liechtenstein, O. Jepsen, and F. Paulsen, J. Phys. Chem. Solids **56**, 1573 (1995)
- [21] K.G. Sandeman and A.J. Schofield, cond-mat/0007299
- [22] A. Hosseini, D.M. Broun, D.E. Sheehy, T.P. Davis, M. Franz, W.N. Hardy, R. Liang, and D.A. Bonn, cond-mat/0312542
- [23] P.V. Bogdanov, A. Lanzara, S.A. Kellar, X.J. Zhou, E.D. Lu, W.J. Zheng, G. Gu, J.-I. Shimoyama, K. Kishio, H. Ikeda, R. Yoshizaki, Z. Hussain, and Z.X. Shen, Phys. Rev. Lett. **85**, 2581 (2000)
- [24] M. Eschrig and M.R. Norman, Phys. Rev. Lett. **85**, 3261 (2000)
- [25] R. Zeyher and A. Greco, Phys. Rev. B **64**, 140510(R) (2001)
- [26] D. Manske, I. Eremin, and K.H. Bennemann, Phys. Rev. Lett. **87**, 177005 (2001)
- [27] M. Eschrig and M.R. Norman, Phys. Rev. B **67**, 144503 (2003)